



# **PACIFIC EARTHQUAKE ENGINEERING RESEARCH CENTER**

## **Rapid Estimation of Ground Shaking for Emergency Response**

**Douglas Dreger**

**Anastasia Kaverina**

University of California, Berkeley

**A report to the PEER Program of  
Applied Earthquake Engineering Research on  
Lifeline Systems**

**The financial support of the sponsor organizations including  
the Pacific Gas & Electric Company (PG&E),  
the California Energy Commission (CEC), and the  
California Department of Transportation (Caltrans) is acknowledged.**

Development of Procedures for the Rapid Estimation of Ground Shaking  
Task 7: Ground Motion Estimates for Emergency Response  
Final Report

Douglas Dreger and Anastasia Kaverina  
University of California, Berkeley, Seismological Laboratory

## **Executive Summary**

This project focused on the development of methodology for the near-real-time estimation of earthquake strong ground motion with the objective of providing this information on a regional (statewide) scale. A critical objective of our development was to provide seamless implementation and uniform performance in varied network coverage. To accomplish this goal we: 1) refined a finite fault inverse method to determine fault slip using regional distance stations; 2) developed a strong motion simulation procedure that uses finite source information as input; 3) investigated the incorporation of site type correction factors, 4) and investigated alternative methods to improve the simulation of high frequency strong ground motions. We have successfully completed these tasks and have developed software that calculates model-based estimates of strong shaking that include the focussing effects due to source directivity. The method we have developed estimates PGA, PGV and spectral acceleration at periods of 0.3, 1.0 and 3.0 seconds. These model predictions may be used to interpolate actual strong motion observations (when available) in the same manner as the southern California TriNet ShakeMap (Wald et al. 1999), and we provide examples of data/model shakemaps for the Landers and Northridge earthquakes. These examples show that it is possible to calculate robust shakemaps even in extremely sparse coverage. In the following the results of each component of the project are summarized.

Under task 1, the refinement of the finite source inverse code largely involved testing and program error fixes to produce stable maps of fault slip using broadband stations located at regional distances. We extensively tested the algorithms with data recorded for the 1992 Landers and 1994 Northridge earthquakes, and compared our regionally derived fault slip maps with those obtained using local strong motion recordings. Favorable comparisons indicate that our methodology is capable of uniquely determining the causative fault plane of the earthquake, the slip dimension (both along strike and down dip), the earthquake rupture velocity, and a reasonable characterization of the gross slip distribution, suggesting that the derived source parameters may be used to simulate near-source strong ground motions. As part of a complementary project we modified the code to facilitate its integration into the Rapid Earthquake Data Integration (REDI) system (Gee et al., 1996) operated by the Berkeley Seismological Laboratory. The codes must still be integrated and tested within the REDI operating environment and we expect that this work will be accomplished in the coming year. Our preliminary testing indicates that the essential source information may be obtained within 4 to 20 minutes following the determination of a seismic moment tensor solution depending upon the level of approximation required.

The focus of task 2 was to use the regionally derived fault slip maps to simulate the distribution of near-source strong ground motion, and to compare the model predictions with observations to calibrate the methodology. Additionally, task 4 involved the testing of hybrid Green's function (Pitarka et al., 1999) and the composite source (Zeng et al., 1994) methods to attempt to better simulate higher frequency ground motions. At the request of the program management committee we also investigated the use of an empirical attenuation relationship that incorporates source specific directivity information (Somerville et al., 1997). For each of the methods we compared predicted values of PGA, PGV and Sa (0.3, 1.0 & 3.0 seconds) against the observations, with the exception of the empirical method because a PGV relationship is not yet available. Our basic method of ground motion simulation is one we developed in which fault slip is deterministically integrated using appropriate local Green's functions. We found that this deterministic approach performed reasonably well in the comparisons of PGV, however the Sa comparisons had mixed results. The PGA, PGV and Sa maps were all found to be successful in outlining the area of observed large ground motions, however there were varying degrees of misfit of the location of predicted and observed maximal values. The methods of Pitarka et al., (1999) and Zeng et al., (1994) improved the results somewhat but not to a degree that offsets their higher computational expense. The glowing success in this project involved the incorporation of the empirical attenuation relationship. PGA and Sa (0.3, 1.0 and 3.0 seconds) were well modeled using the approach of Somerville et al. (1997), which utilized the regionally derived finite source information as input. The empirical approach is also extremely fast and requires information available after the initial fault plane and rupture velocity inversion, which is also relatively fast. The best shakemaps for the two study events were obtained by taking the larger of the two values from the deterministic and the empirical maps. We call this map our 'conservative shakemap'. The empirical component of the conservative shakemap is found to explain the mean attenuation of the observed strong motions very well and the deterministic component provides a better estimate of the large near-fault ground motions.

Under task 3 we explored ways to improve the predicted strong motion parameters by applying site corrections to the synthetic ground motions. To facilitate this comparison we utilized the methodology implemented by Wald et al. (1999) for the southern California TriNet ShakeMap. In this case the site geology is classified as quaternary, tertiary and Mesozoic (QTM), and site corrections after Borchardt (1994) are applied. We found that the QTM corrections improved the agreement with the observations but not enough to offset a systematic under prediction at LA basin sites. A second method used two 1D velocity models to characterize rock and soil sites. The application of site specific Green's functions provided a noticeable improvement in the predicted shakemap. However we note that stations located within the LA Basin remain under predicted. The results show that empirically derived site corrections applied to synthesized time histories is not enough to offset the effects due to large scale 3D structures such as the LA basin. It may be possible to determine site adjustments for specific 1D velocity models numerically using finite difference methods and appropriately calibrated 3D structure models to develop a table of 3D-to-1D site adjustments. This can presently be accomplished in southern California and the San Francisco bay area, however in large regions of central and northern California such a calibration would require a very considerable effort to compile and verify a suitable 3D structure model.

Through the course of this research we have developed a multi-staged algorithm to generate a shakemap. First, line source or course planar inversions are performed to determine the rupture velocity, causative fault plane and slip dimension of an earthquake. This information may then be used to generate a shakemap using a directivity sensitive attenuation relationship (e.g. Somerville et al. 1997). Site adjustments are applied to the empirical rock ground motions. This stage of processing may only consume 4 to 15 minutes of CPU time depending upon the level of approximation. Strong ground motion parameters that may be estimated at this stage include PGA and spectral acceleration at 0.3, 1.0 and 3.0 seconds period. It will be necessary to develop a directivity sensitive PGV attenuation relationship to provide a seamless methodology. If local strong motion data is available it may be integrated with the empirical values to develop a data/model shakemap. With relatively dense coverage the map would be data driven with model predictions contributing only in the regions where there are gaps in coverage. Following the determination of the causative fault plane and rupture velocity, processing may be continued to determine a higher resolution picture of the distribution of fault slip. This additional processing step consumes an additional 18 minutes for both of the earthquakes we studied. The higher resolution slip map is then used to simulate near-source synthetic time histories from which values of PGA, PGV and spectral acceleration may be measured. We then combine the larger of the simulated and the empirical ground motions to produce a 'conservative shakemap'. As in the first stage of processing available data may be integrated into the shakemap, where model predictions are used to interpolate only in areas where there are no observations. Using the attenuation relationship as an integral component of the methodology allows various levels of approximation such as the use of a strong motion centroid with point-source attenuation (e.g. Wald et al., 1999), source directivity specific empirical attenuation, and finally the source directivity specific 'conservative shakemap' developed in this study. A common multi-parametric attenuation relationship provides seamless transition from one level of approximation to another as more data and model information becomes available. We conclude this report with examples of the evolution of a shakemap for the Northridge and Landers earthquakes in very sparse network coverage as may be anticipated in large areas of California and the western United States.

## Introduction

Earthquake information available soon after a damaging earthquake begins with estimates of the time of occurrence, the epicenter and hypocenter, an estimate of the magnitude, and fairly recently a seismic moment tensor solution providing a more robust estimate of earthquake size and the radiation pattern (e.g. Pasyanos et al. 1996). While such basic information is essential in the rapid characterization of the likely damage due to strong ground motions from the earthquake it is a rather limited characterization. Ideally city and state emergency response providers, public utilities and earthquake engineers would like to know where the strongest shaking occurred, which in a large extended earthquake is very likely not co-located with the epicenter.

In southern California this problem has been addressed with the development of the TriNet network of broadband and strong motion instruments that provide digital data in near real-time. The TriNet calls for the installation of 600 digitally recorded accelerometers to monitor strong ground motions throughout southern California, with the greatest density of coverage in the urban area. Figure 1 shows the locations of TriNet stations that are in the ground and compares the monitoring regions of both southern and northern California. These stations are currently being used to rapidly contour the regional extent of strong ground shaking (Wald et al., 1999). Parameters relevant to emergency response providers, utilities and engineers such as peak ground acceleration (PGA), peak ground velocity (PGV) and, spectral acceleration at periods of 0.3-1.0-3.0 s, and instrumental intensity are automatically determined and posted to the WWW. Additionally, seismological information such as first-motion focal mechanisms and seismic moment tensors are also provided. Figure 2 compares TriNet PGV shakemaps for the Northridge and Landers earthquakes. In the case of the Northridge earthquake (Figure 2b) the station coverage is quite good and there is considerable definition of the shakemap contours. The region of elevated PGV north of the epicenter is due to directivity focusing and the region northeast of the epicenter is due to both directivity and basin amplification. In contrast the station coverage for the 1992 Landers earthquake is sparse and the fortuitous location of the Lucerne Valley station is controlling the mapping of PGV near the fault.

In northern California there are plans to develop a TriNet like system, however because the monitoring area in northern California is considerably larger and a northern California TriNet is only in its conceptual phase, interim methods and methods suitable for sparse networks need to be developed. The distributed nature of at risk facilities is demonstrated by the locations of the dense urban areas of the San Francisco Bay and Sacramento, hydroelectric power generation facilities, rail transportation, state and national public highways, and the state aqueduct system. Thus a shakemap system for central and northern California needs to provide rapid estimates of strong shaking in the urban areas as

## Broadband and strong motion coverage

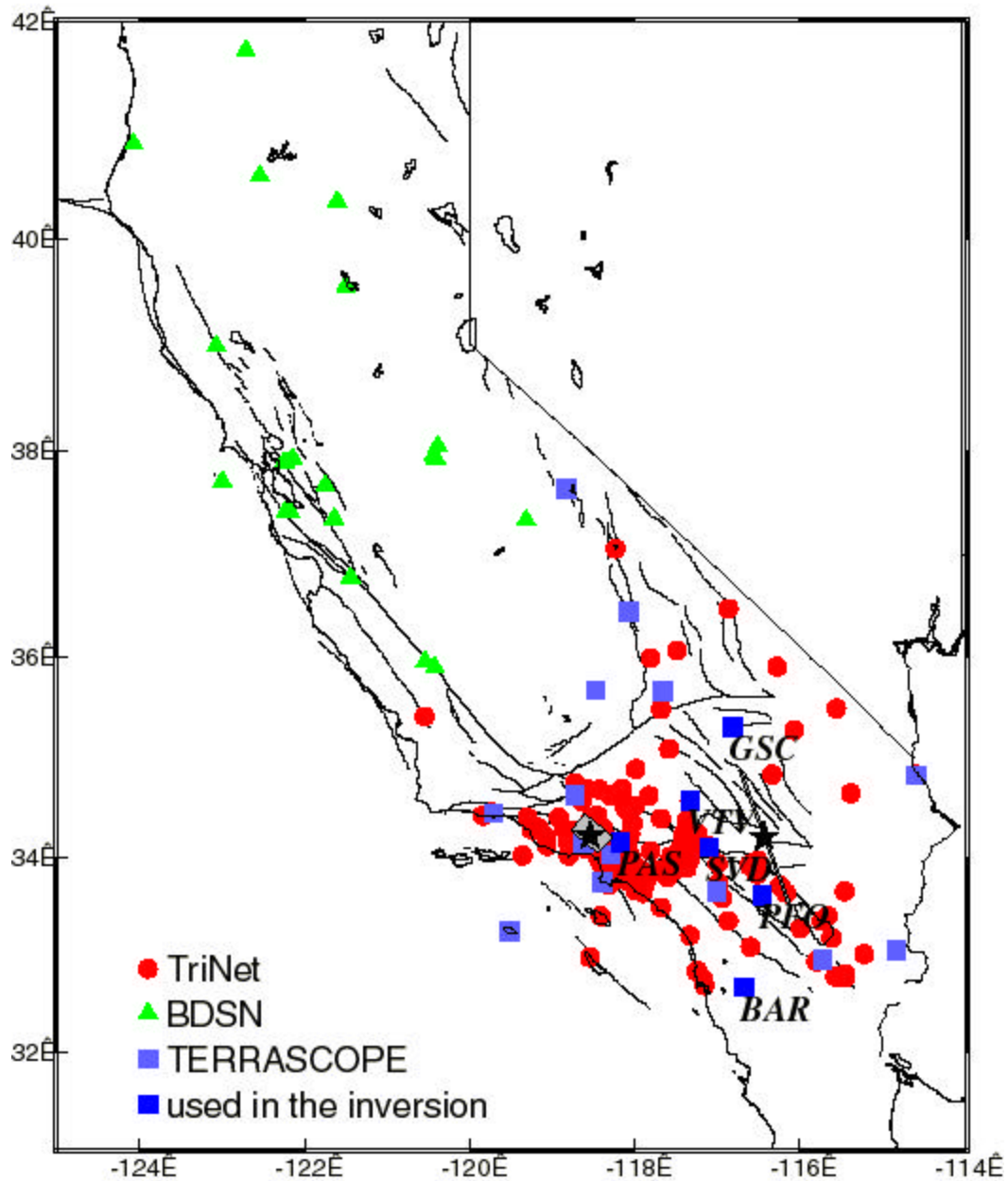
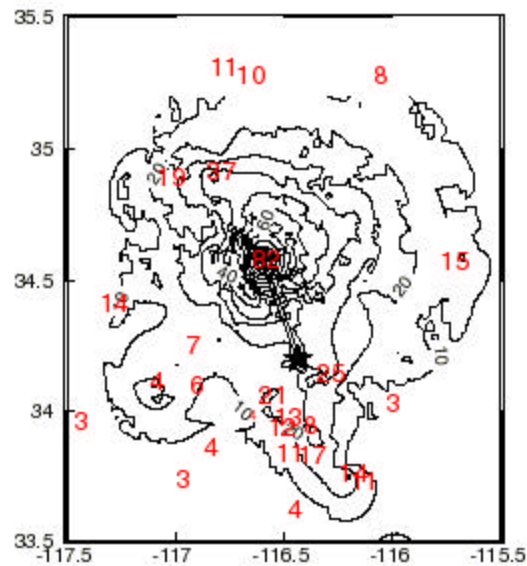


Figure 1. Map showing broadband and strong motion coverage in southern California. The red circles show strong motion stations of the TriNet, and the blue squares show broadband TERRAScope stations. The broadband Berkeley Digital Seismic Network (green triangles) compares the broadband coverage in central and northern California. Stations that were used in our analysis are identified by name.

well as the surrounding rural areas where most of the supporting infrastructure is located. The focus of this research project is to develop such a system that simulates near-source strong ground motions using event specific source information derived from the regional Berkeley Digital Seismic Network (BDSN, Figure 1). The BDSN is a continuously recording and digitally telemetered network with co-sited weak and strong motion sensors. The data latency of this system is minimal and data from this system is used to locate, estimate magnitude, and provide strong motion values for earthquakes in near-real-time (Gee et al., 1996). The data from this network is further used to determine the seismic moment tensor of  $M > 3.5$  earthquakes throughout central and northern California in near-real-time (Pasyanos et al., 1996). The software and methodology we have developed under this contract naturally builds on the automatic processing that has already been implemented. In this study we test the new methods using regional and broadband data sets collected for the June 28, 1992 Landers ( $M_W 7.1$ ) and the January 16, 1994 Northridge ( $M_W 6.7$ ) earthquakes.

### Landers Trinet ShakeMap, PGV



### Northridge Trinet ShakeMap, PGV

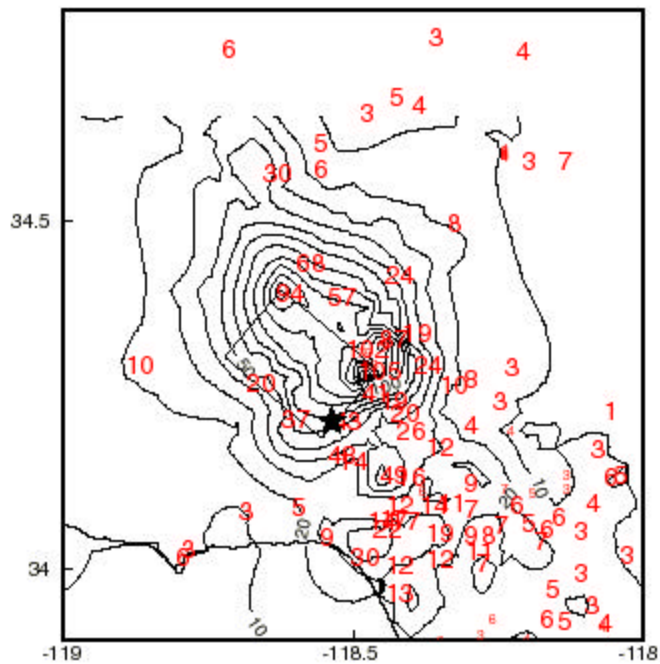


Figure 2. TriNet PGV shakemaps are compared for the 1992 Landers (a) and the 1994 Northridge (b) earthquakes. The contours show TriNet shakemap values and the red numbers show the observed PGV at individual recording stations. Both are in units of cm/s. Note that only the stations shown were used in the determination of the shakemap contours, however an attenuation model scaled from the observed strong motion centroid was used to help interpolate the map where data does not exist (e.g. Wald et al., 1999). The stars identify the epicenters.



## Section I: Regional Distance Finite Fault Determination

Following the occurrence of an earthquake in central and northern California there is a hierarchy of information that is determined by the UCB/USGS Joint Notification System. Earthquake locations are obtained within several minutes. Broadband waveform data recorded by the BDSN is used to estimate a local magnitude ( $M_L$ ) and if the  $M_L$  is greater than 3.5 a seismic moment tensor is determined. Typically the seismic moment tensor is obtained within 6-9 minutes after the occurrence of an earthquake. The seismic moment tensor inversion provides estimates of the scalar seismic moment, a centroid depth and the orientations of two possible fault planes. The point-source representation used in the seismic moment tensor method results in a fault plane ambiguity. The ability to rapidly determine the causative fault plane is of value in itself to understand the possible extent of damage following an earthquake. We have modified a method to determine earthquake finite source parameters (fault slip, dislocation rise time and rupture velocity) to use regionally recorded broadband waveforms. In this method, given a hypocenter location and a source mechanism of an earthquake, we use a non-negative least squares solver to determine the distribution of fault slip from regionally recorded broadband data. This method is similar to those used to invert local strong motion data for earthquake source parameters (e.g. Cohee and Beroza, 1994; Wald and Heaton, 1994). In the source model, the rupture propagates with constant velocity over a grid of point sources each with constant dislocation rise time, and the Green's functions are shifted in time to account for relative hypocenter-subfault-station distances and the time for the passage of a circular rupture front. We use a precompiled catalog of Green's functions for point source responses. The Green's functions are computed using a frequency-wavenumber approach developed by Saikia (1994) and must be computed in advance since this preparatory step is very time consuming. The velocity model we use to estimate the source parameters is SoCal (Dreger and Helmberger, 1993), which has been found to be an appropriate representation of average crustal properties throughout southern California. The implementation of the procedures described in this report in central and northern California will require a different set of Green's functions. The central and northern California region may be approximated by both the SoCal and the GIL7 velocity models (Dreger and Romanowicz, 1994; Pasyanos et al., 1996). Because of the regional nature of the inverse problem we are solving we simplify the problem by considering only constant values of dislocation rise time and rupture velocity. In addition we assume that the rake angle of individual subfaults is constant and equal to average value obtained from automatic moment tensor analysis.

The code we have developed solves the following system of linear equations subject to non-negativity in slip, slip smoothing, fault edge damping.

$$\begin{bmatrix} \frac{A}{I \cdot S} \\ E \end{bmatrix} \bullet [U] = \begin{bmatrix} d \\ 0 \\ 0 \end{bmatrix}$$

$A$  is a matrix of Green's functions,  $S$  is a smoothing matrix with relative weight,  $I$ ;  $E$  is a matrix defining the edges of the distributed fault plane.  $U$  is the slip that is solved for and  $d$  is the input broadband waveform data. The smoothing ( $S$ ) and fault edge ( $E$ ) parameters are included to damp the inversion minimizing slip roughness and edge slip, respectively.

The inverse procedure begins by testing the two possible fault planes determined from the seismic moment tensor analysis. In order to do this it is necessary to scale the inverse problem to the size appropriate for the reported scalar seismic moment. This is accomplished by using the empirical relationships of Wells and Coppersmith (1994) for fault dimension, doubling them to allow for bilateral rupture and increasing them by 20% to be safe. To determine the appropriate dislocation rise time to use we assume that the rupture velocity is 80% of the local shear wave velocity and that the total duration of the earthquake is equal to the fault dimension divided by the rupture velocity. The dislocation rise time is assumed to be 10% of the approximate total duration after Heaton (1990). For the Landers and Northridge earthquake values of 3.7s and 1.4s are obtained by this method and are found to be reasonable in view of reported values for these respective earthquakes. Given the overall dimension of the distributed fault and the assumed dislocation rise time the two possible fault planes are tested by performing separate inversions over a range of rupture velocity. To speed up this process and to minimize computer load the code has the option of using either a line source representation of the source or a planar fault with relatively large subfaults. The best solution is the one that maximizes the variance reduction,

$$VR = \left( 1.0 - \frac{\sum (d_i - s_i)^2}{\sum d_i^2} \right) \bullet 100,$$

where  $d$  and  $s$  are the observed and synthetic waveform, respectively, and  $i$  is a time index. Once the causal fault plane and rupture velocity are found the inversion is performed once more with a higher resolution to better characterize the fault slip.

We have found that it is possible to determine finite source parameters that compare quite well with those obtained using local strong motion records. Figure 3 compares slip maps for the January 16, 1994 Northridge earthquake obtained using strong motion records (Wald et al., 1996 and Zeng and Anderson, 1996) with those obtained at regional distances using an empirical Green's function method (Dreger, 1994, 1996) and using theoretical Green's functions (this study). It is clear that the slip maps are very similar suggesting that the regionally derived maps may be used to estimate the level of shaking in the near-source region. We obtain an equally impressive comparison for the Landers earthquake.

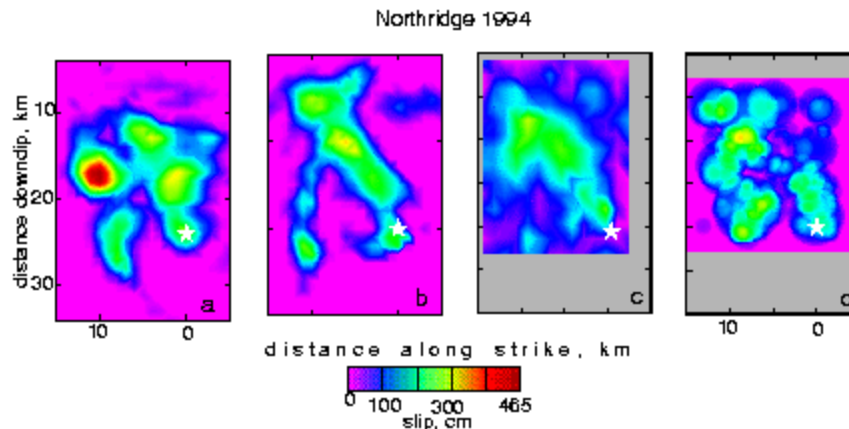


Figure 3. Fault slip maps for the 1994 Northridge earthquake are compared. (a) The slip map obtained in this study by inverting regional distance broadband data. (b) The slip map obtained by inverting seismic moment rate functions derived from empirical Green's function deconvolution (Dreger, 1994; Dreger, 1997). These maps compare well with those obtained by inverting local strong ground motions. (c) compares the map of Wald et al. (1996) obtained from local strong motion, teleseismic waveform data, and geodetic and leveling data. (d) Zeng and Anderson (1996) inverted only strong motion data using a different methodology. Each map has the same scaling and the white star identifies the hypocenter.

### Landers Earthquake Application

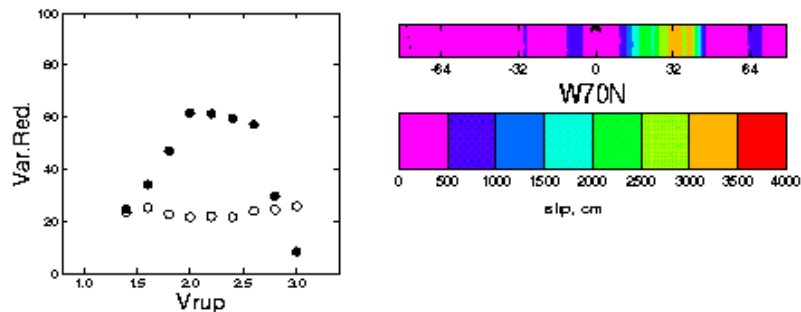
Four TERRAscope stations, GSC, PAS, PFO and SVD (Figure 1) were used to determine the slip for the Landers earthquake. Figure 4a shows the best line source inversion results and the variance reduction plotted as a function of rupture velocity. In this case the northwest striking nodal plane is found to fit the data much better than the east west striking nodal plane that results in a flat variance reduction curve. The line source results show that slip is unilateral to the north-northwest. The total calculation time for all 18 rupture velocities tested was 3.5 minutes. This line source run is quite rapid and derives the necessary information for the implementation of a shakemap based on directivity sensitive empirical attenuation relationships (e.g. Somerville et al., 1997). Such an implementation will be discussed in a later section of the report. Figure 4b shows the high-resolution inversion results. In this case the model is found to be unilateral with the bulk of slip being located approximately 50-km north-northwest of the hypocenter. Furthermore, the slip is found to be relatively shallow, although the inversion was allowed to place slip as deep as 25 km if required by the data. The total processing time for the high resolution run was 18.5 minutes.

The source models shown in Figure 4 do not include a 2.5 s delay in the start of significant rupture reported by several researchers (Abercrombie, 1994; Cohee and Beroza, 1994; Dreger, 1994b; Wald et al., 1994). Furthermore the Landers earthquake also involved rupture of multiple segments with a 35-degree variation in fault strike (Wald et al., 1994). With automatic processing it will not be possible to take this level of complexity into account. Nevertheless the slip distribution we obtain with a single fault plane compares well with the multi-planar results of Wald et al. (1994) when their slip is projected onto our fault plane, and

we consider the 2.5s delay in our inversion for fault slip. In a later section of the report we demonstrate that although we have significantly simplified the source model of Landers it is still possible to obtain a shakemap with good agreement to the data, and excellent results when both data and model predictions are combined.

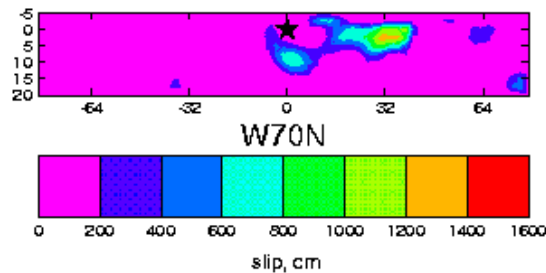
## Landers, Mw 7.3

### I. Loop over rupture velocity (line source approximation)



Calculation time 3.5 min; 65 subfaults; 12 components of data

### II. Full resolution for the best Vrup (2.0 km/s)



Calculation time 18.5 min; 715 subfaults; 12 components of data

Figure 4. (I) The variance reduction versus rupture velocity is plotted for both possible nodal planes for the Landers earthquake using a line source model parameterization. The solid circles show variance reduction values for the north-northwest striking plane and the open circles show values for the conjugate east-west striking plane. This example clearly shows that the north-northwest plane provides a superior fit to the data. The best line source slip distribution is shown to the right and results in unilateral rupture to the north-northwest. (II) The full resolution inversion results are compared to the line source result.

## **Northridge Earthquake Application**

Five TERRAscope stations, BAR, GSC, PFO, SVD, and VTV (Figure 1) were used to determine the slip for the Northridge earthquake. Figure 5 compares a low-resolution planar fault inversion with a high-resolution inversion for the Northridge earthquake. As the variance reduction vs. rupture velocity plot shows there is not as much separation between the two possible fault planes as was found for Landers. This is function of the relative size and the type of earthquake. The Landers earthquake being larger and strike-slip produces a stronger horizontal directivity function than the smaller reverse-slip Northridge earthquake. Nevertheless, as the variance reduction plot shows the south dipping fault plane is correctly identified for Northridge. The total calculation time for the 18 rupture velocities tested was 15 minutes. The high-resolution run produces additional complexity in the slip distribution. The total processing time for the high resolution run was 17 minutes. Figure 3 shows that the results are very similar to those obtained using local strong motions.

## **Section I: Conclusions and Recommendations**

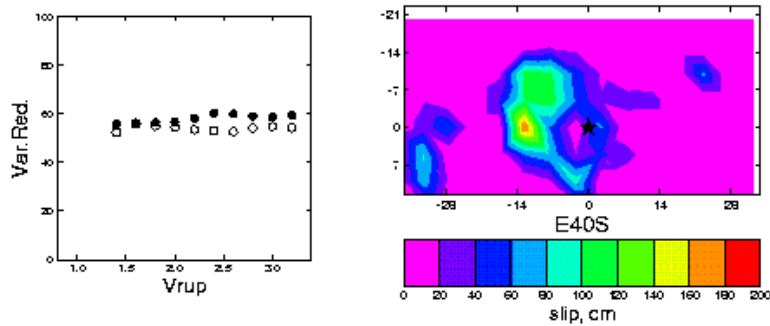
Our application of a regional distance finite fault inverse methodology to TERRAscope broadband data for the Landers and Northridge earthquakes reveals that the obtained slip models compare well with those obtained by inversion of local strong motion waveforms. The comparisons indicate that the regional estimates of fault dimension, gross slip distribution and directivity are reasonably well determined for these earthquakes. In the next section we demonstrate that near-source strong shaking determined from these slip maps models the observed strong shaking fairly well.

The calculations we have performed under this contract were carried out on a SUN Enterprise server with 400MHz CPUs. These systems are relatively standard and faster workstations are now becoming available indicating that the process times of the various steps that we have outlined are likely to be significantly reduced in the future.

At the time of the Landers earthquake six TERRAscope stations were available. The four that we used are located in vaults on relatively competent material. The ISA station was not used because of non-standard orientation of the horizontal components. The SBC station was not used because the path from Landers to San Barbara crosses significant basin structures and the 1D models that we employ are not adequate to explain the complex seismograms (Dreger and Helmberger, 1991). It is noted however that for the Northridge earthquake a number of the stations that we use do traverse the Los Angeles basin and the 1D structure appears to perform well. The implementation of this stage of processing will certainly require the careful calibration and verification that the 1D-velocity models employed are reasonable estimates of average path structure, and some regional stations with substantial site effects should be removed from processing to minimize possible bias due to unmodeled Earth structure.

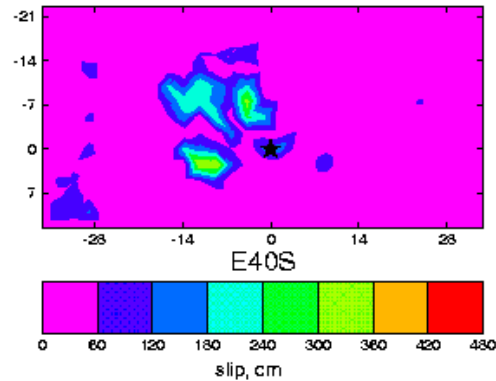
## Northridge, Mw 6.7

### I. Loop over rupture velocity (low resolution)



Calculation time 15 min; 120 subfaults; 12 components of data

### II. Full resolution for the best Vrup (2.4 km/s)



Calculation time 17 min; 435 subfaults; 12 components of data

Figure 5. (I) The variance reduction versus rupture velocity is plotted for both possible nodal planes for the Northridge earthquake using a low resolution planar model. The solid circles show variance reduction values for the best fitting south dipping plane and the open circles show values for the conjugate north-dipping plane. The best low-resolution plane slip distribution is shown to the right, and shows northward updip directivity. (II) The full resolution inversion results are compared to the low-resolution result.

## Section II. Near-Source Shakemap Simulation

Given a representation of the earthquake specific slip distribution it becomes possible to integrate the slip both spatially and temporally for stations located above the source to generate a suite of near-source time histories from which to determine strong motion parameters such as PGA, PGV and spectral acceleration. We keep the parameterization in the forward problem simple by assuming that the rupture velocity and the dislocation rise time are

constant throughout the rupture. The rupture velocity obtained from the source inversion is used and the dislocation rise time is determined from the derived slip, rupture velocity and the observations of Heaton (1990). The values of dislocation rise time used in this step are 2.4s and 0.9s for the Landers and Northridge earthquakes, respectively. These values are consistent with those previously reported for these earthquakes. In the following we compare our predicted PGV and spectral acceleration maps with observations from both the Landers and Northridge earthquakes. Our predicted shakemaps utilize site specific Green's functions calculated from two velocity models, one for hard rock and the other for soft rock. These velocity models are shown in Table 1 and were used by Wald et al. (1996) to invert for Northridge fault slip. In a later section we illustrate the benefit of using the two 1D models to account for site variability.

Table 1a: Hard Rock Velocity Model

$V_P$ (km/s)	$V_S$ (km/s)	Density (g/cm <sup>3</sup> )	Depth (km)
1.9	1.0	2.1	0.0
4.0	2.0	2.4	0.5
5.5	3.2	2.7	1.5
6.3	3.6	2.8	4.0
6.8	3.9	2.9	27.0
7.8	4.5	3.3	40.0

Table 1b: Soil Velocity Model

$V_P$ (km/s)	$V_S$ (km/s)	Density (g/cm <sup>3</sup> )	Depth (km)
0.8	0.3	1.7	0.0
1.2	0.5	1.8	0.1
1.9	1.0	2.1	0.3
4.0	2.0	2.4	0.5
5.5	3.2	2.7	1.5
6.3	3.6	2.8	4.0
6.8	3.9	2.9	27.0
7.8	4.5	3.3	40.0

### Deterministic Peak Ground Velocity (PGV) Maps

Predicted and observed PGV for the Landers earthquake are compared in Figure 6. The predicted values were computed with site specific Green's functions in the 0.1 to 1.0 Hz pass band. In Figure 6a contouring was done for predicted values at the same locations as the observations, and the shape of the contours is an artifact of the station geometry. This PGV map compares well with the one obtained by the TriNet ShakeMap system (Figure 2a). Figure 6b compares the contours for a dense grid of stations, and shows an elongate region of high PGV close to the fault as would be expected for an extended fault rupture such as Landers. The site specific calculation shows our best results for Landers and it is evident that we are over predicting the PGV at the Lucerne station (LUC) by a factor of two. In contrast the hard rock prediction (Figure 6b) is much better at LUC. Other stations relatively close to the fault are well modeled however. There could be a number of factors such as inappropriate site

classification, problems with the Green's functions, and most likely the artificial closeness of the fault that could be causing the over prediction at LUC. The fault from our single plane model passes within 0.3 km of LUC while the closest mapped trace is approximately 3 km away. In fact a calculation that takes the curvature of the Landers fault into account results in much better estimates at LUC. Unfortunately this level of complexity can not be done automatically. Figure 6c shows the comparison of PGV as a function of distance. The predicted values span the range observed in the data and describe the attenuation of PGV with distance quite well. The cluster of large amplitude observations at a distance of approximately 150-km is from stations located in the Los Angeles basin.

Predicted and observed PGV for the Northridge earthquake are compared in Figure 7. The predicted values were computed with site specific Green's functions in the 0.1 to 1.0 Hz pass band. The observed PGV were computed by integrating the accelerograms and band pass filtering the derived velocity seismograms in the 0.1 to 1.0 Hz pass band, and picking the maximum value. The PGV map (Figure 7a) is successful in the characterization of the region that experienced the largest ground motions (PGV>10 cm/s). The map further shows that elevated PGV are predicted north of the epicenter due to updip rupture directivity, which is consistent with observation. Both over and under prediction is observed in the forward directivity region, and these discrepancies are likely to be due to a combination of the simplified source model obtained from regional distance data, site variability in observed PGV, and the use of simplified 1D velocity models. Figure 7b shows that the predicted values describe the attenuation very well, however there is a systematic under prediction of PGV at sites located in the Los Angeles basin (distance range of 30 to 150 km in Figure 7b).



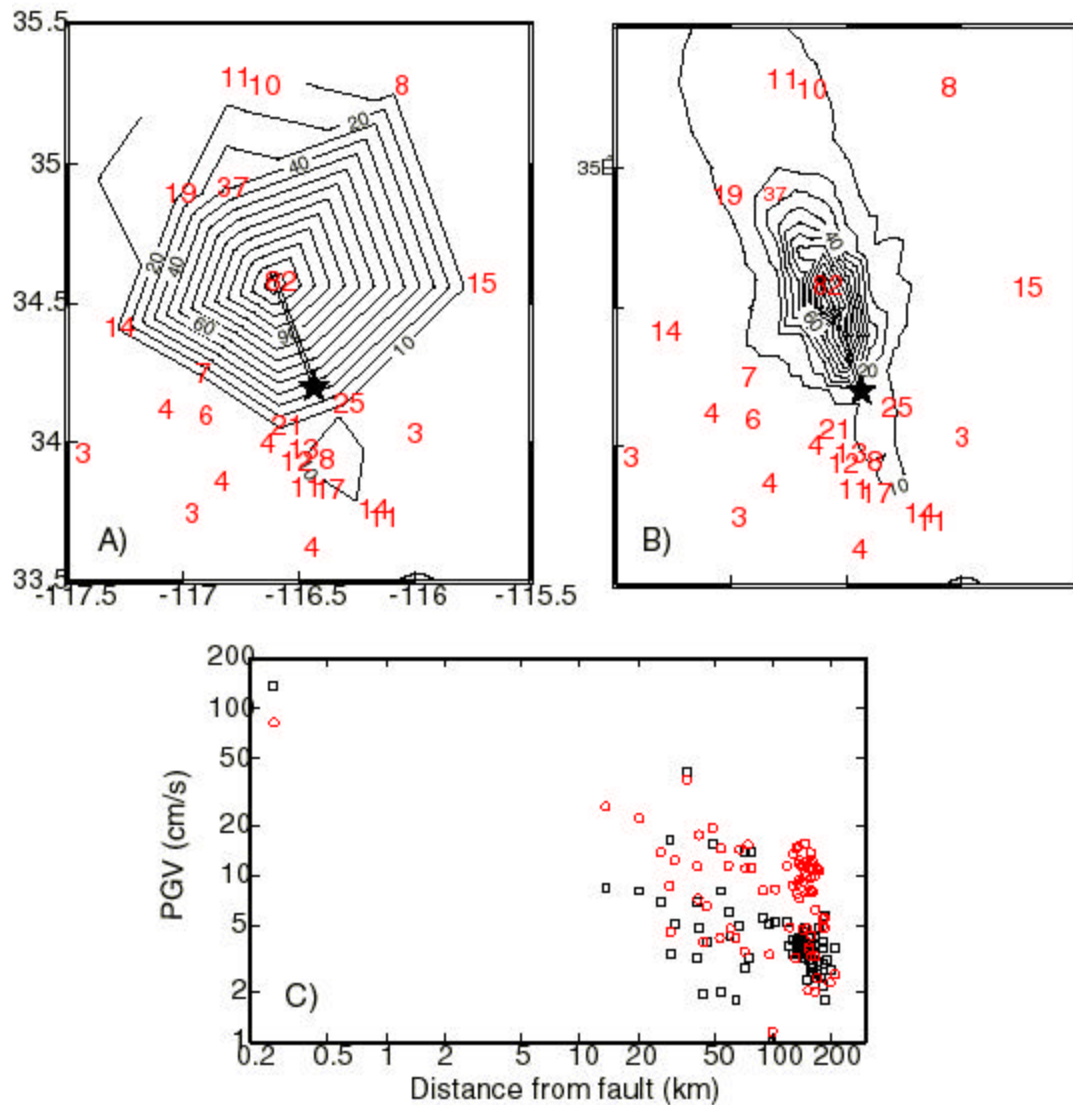


Figure 6. (a) Comparison of predicted (contours) and observed (red numbers in cm/s) PGV for the Landers earthquake. Both the predicted and observed PGV were determined from the 0.1 to 1.0 Hz pass band. The predicted PGV were measured from synthetic time histories generated using site specific Green's functions (see Table 1). (b) PGV contoured from a dense distribution of stations using hard rock Green's functions. (c) Log-log plot comparing observed PGV (red circles) and predicted values (black squares). The predicted values are for the site specific calculation shown in (a). The cluster of elevated observed ground motions at a distance of 150 km are from sites located in the Los Angeles basin southwest of the area shown in (a).

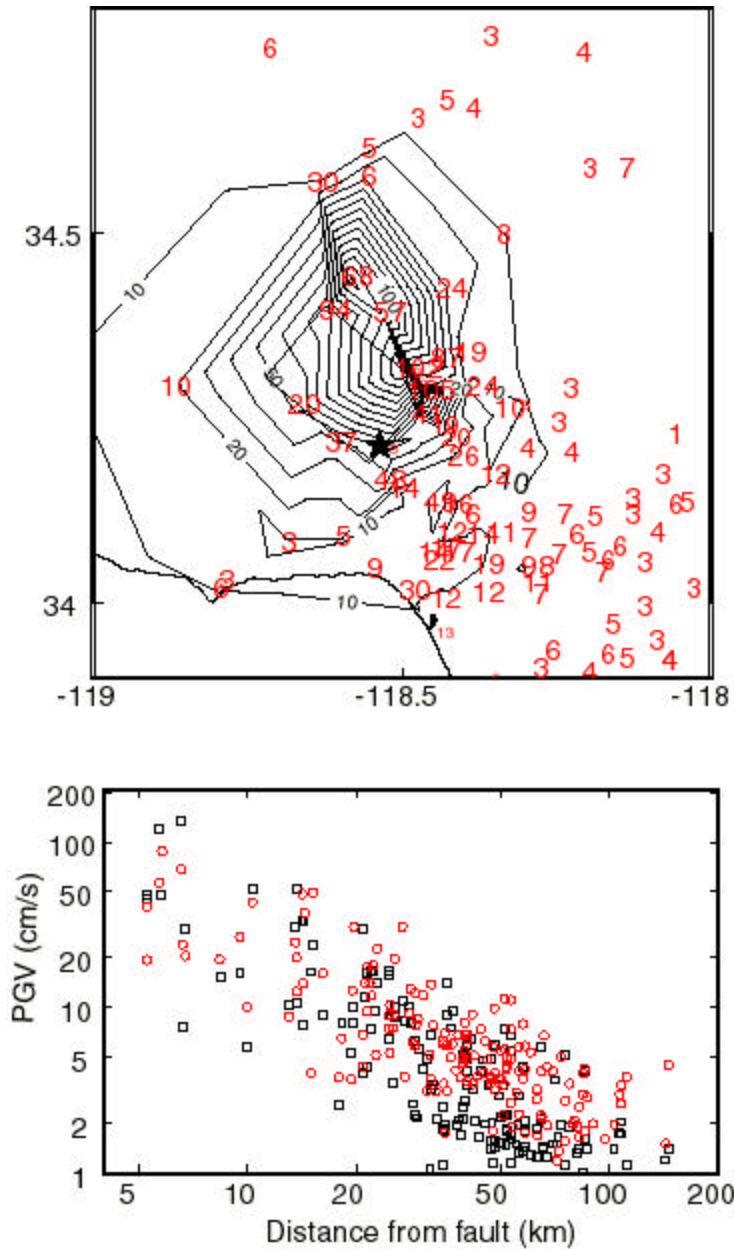


Figure 7 (a) Comparison of predicted (contours) and observed (red numbers in cm/s) PGV for the Northridge earthquake. Both the predicted and observed PGV were determined from the 0.1 to 1.0 Hz pass band. The predicted PGV were measured from synthetic time histories generated using site specific Green's functions (see Table 1). (b) Log-log plot comparing observed PGV (red circles) and predicted values (black squares). The predicted values are for the site specific calculation shown in (a). PGV is under predicted at LA Basin sites in the 30 to 150 km distance range.

## **Deterministic Spectral Acceleration Maps**

Spectral acceleration (Sa) at 0.3, 1.0 and 3.0 seconds period was determined from the simulated time histories for both earthquakes. Figure 8 compares the predicted and observed Sa for the Northridge earthquake for the three specific periods. In this comparison the site specific Green's functions were used. The map view comparison is fairly good in that elevated regions of Sa are distinguished from areas with low relative Sa. For example in the 0.3 second plot the maximum observed Sa of 2.1 g correlates well with the predicted maximum although the predicted value of 2.8g is too large. In contrast stations to the southeast in the LA basin have relatively lower Sa. In the 1.0 second Sa plot the 0.1g contour separates the regions of higher and lower observations. The best agreement is for the 3.0 second Sa map. Figure 8b compares observed and predicted Sa as a function of distance, where the scatter in the data and the attenuation of Sa are well modeled. The 1.0 and 0.3 second distance plots (Figure 8b) tend to show that the model under predicts Sa in the 30-150 km distance range primarily for LA basin sites.

As was the case for Northridge the predicted Sa for Landers defines the region of strongest shaking, however there is a general under prediction. 3.0 second period Sa at LUC is significantly over predicted while the 1.0 second and 0.3 second period Sa are significantly under predicted. Part of the misfit is likely to be due to the artificial closeness of LUC to the model fault. The fact that some periods are over predicted and others under predicted and the general under prediction of Sa for all distances suggests that there is a problem in the spectral content of the simulated time histories. It is curious however that the PGA and PGV maps for Landers compare with the observations fairly well. Further study is needed to explore the sensitivity of the simulated time histories and estimated PGA, PGV and Sa to slip model, Green's function, site response, and rupture velocity and dislocation rise time uncertainty as well as simulation methodology. We tested the methods of Pitarka et al. (1999) and Zeng et al. (1994) and found minimal improvement for Northridge. It may be worthwhile to test their methods in simulating Sa for Landers. It is noted however that the empirical attenuation relationship described in the next section significantly improves the predicted Sa at all three periods.

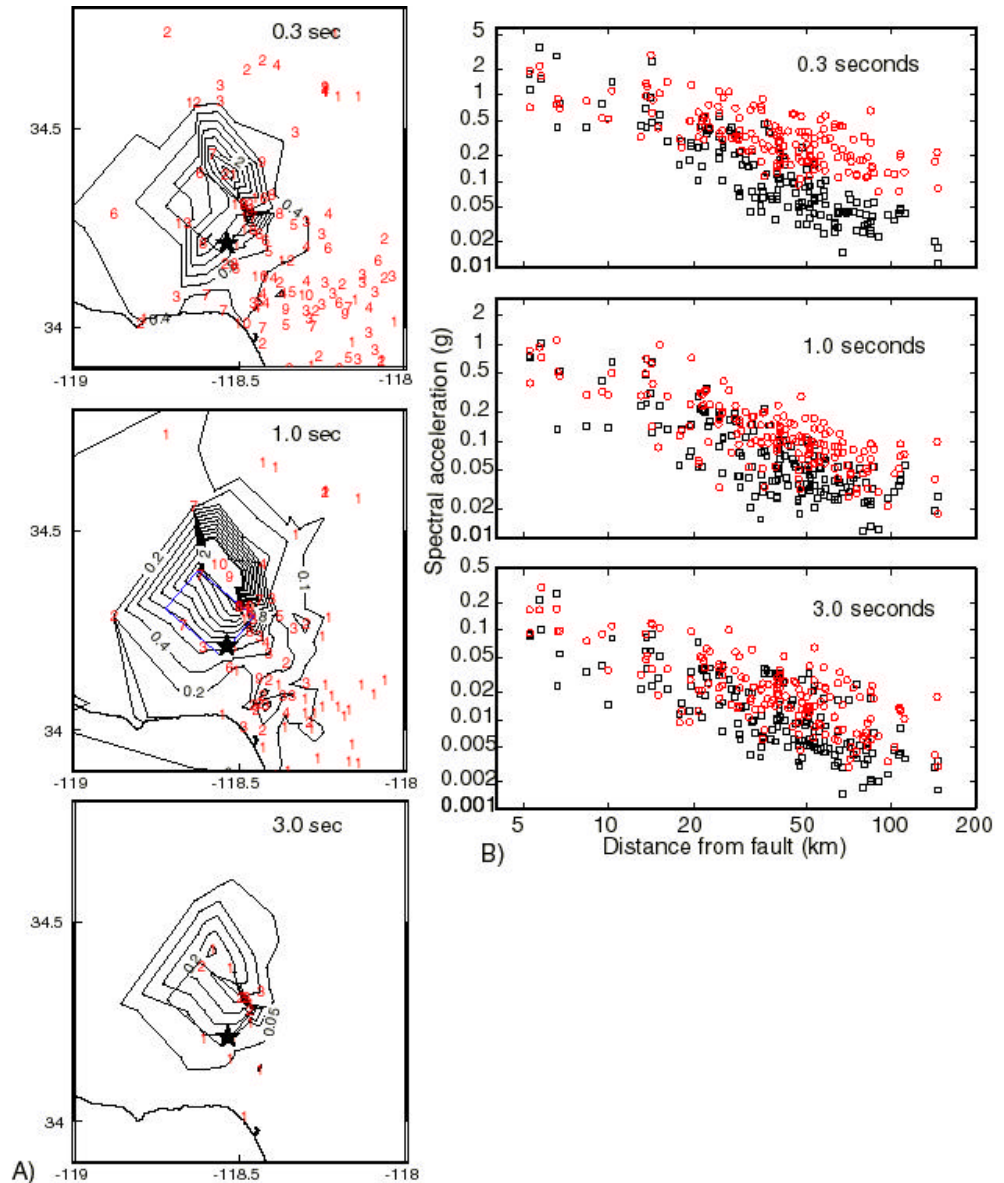


Figure 8. (a) Spectral acceleration at 0.3, 1.0 and 3.0 seconds period is compared for the Northridge earthquake. Contoured values were obtained by simulation using the Northridge slip model (Figure 3a) and site-specific Green's functions (Table 1). Contours are in 0.4, 0.2 and 0.05g intervals for the respective periods, and were constructed from predicted values only at the locations of the recording stations that are shown. The observed values (red numbers) are given in tenths of a g. Only observed values above 0.1g are plotted. (b) The predicted (black squares) and observed (red circles) spectral acceleration is compared as a function of distance for the three periods.

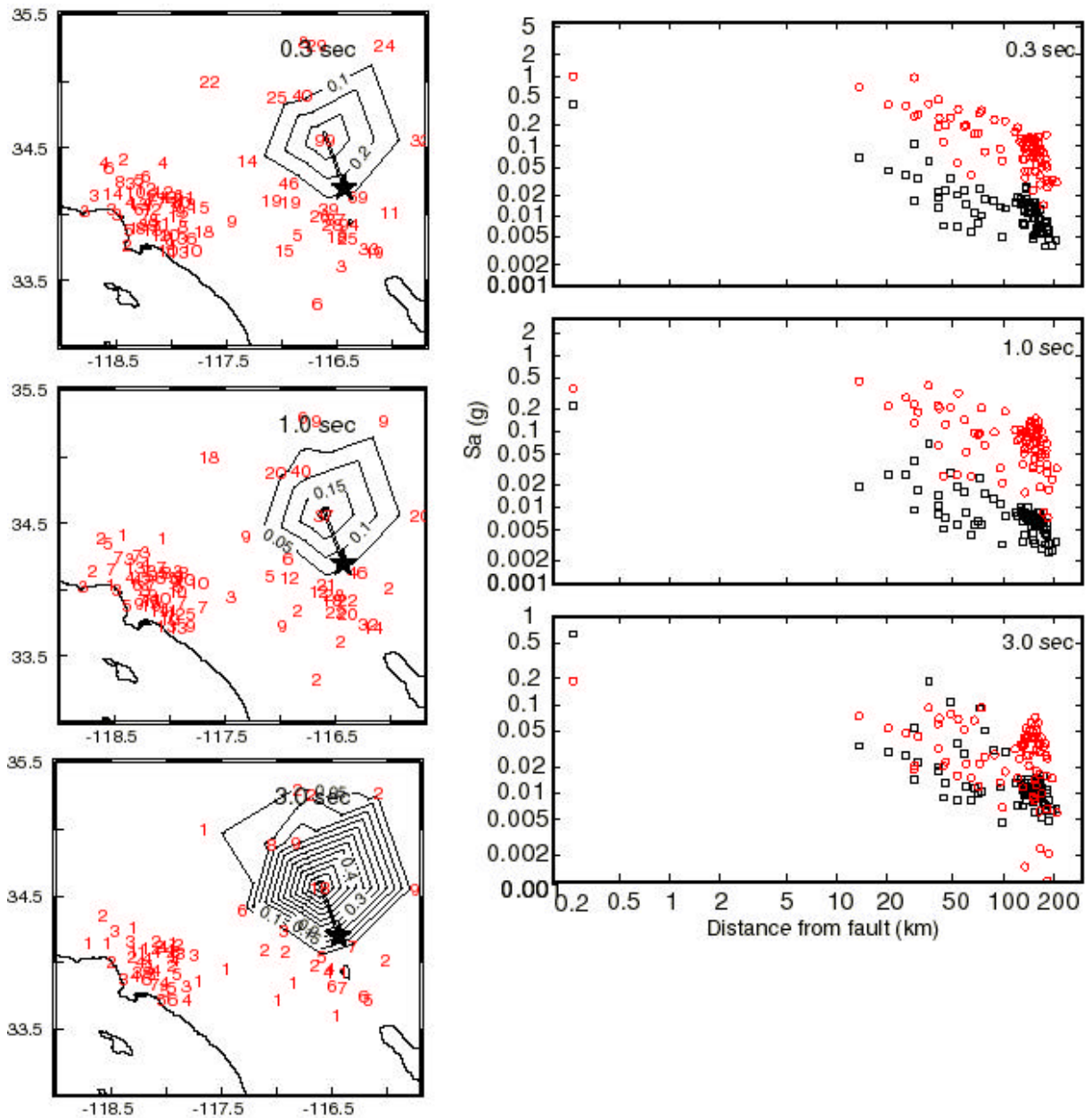


Figure 9. (a) Spectral acceleration at 0.3, 1.0 and 3.0 seconds period is compared for the Landers earthquake. Contoured values were obtained by simulation using the Landers slip model (Figure 4II) and site specific Green's functions. Contours are in 0.4, 0.2 and 0.05g intervals for the respective periods. The observed values (red numbers) are given in hundredths of a g. Only observed values above 0.01g are plotted. (b) The predicted (black squares) and observed (red circles) spectral acceleration is compared as a function of distance for the three periods.

## **Empirical Spectral Acceleration Maps**

A recently developed directivity sensitive attenuation model (Somerville et al., 1997) was used to simulate PGA and Sa at 0.3, 1.0 and 3.0 seconds period. This model takes the scalar seismic moment, fault orientation, and slip distribution that we obtain by our source inversion as input. The empirical model describes the mean attenuation observed for the Landers earthquake (compare figures 10a to 9b), and is a significant improvement over the deterministic Sa shown in Figure 9. For the Northridge earthquake the empirical relationship also describes the observed mean attenuation, although at near-distances it under predicts the Sa.

If one integrates the maximum predicted values from the deterministic and empirical models a conservative map is obtained (Figure 11). This map is found to provide the best agreement to the data. The empirical model provides a mean value estimate for stations at all distance ranges and the deterministic calculation contributes mostly in the very near source distance range where source specific information is important.

In the case of Landers the conservative 0.3 and 1.0 second Sa shakemaps are a big improvement and stations close to the fault have values close to those indicated by the contours. LUC is now slightly over predicted which is likely to be due to the artificial closeness of the station to the model fault. The 3.0 second map is not changed very much. For Northridge there is some improvement particularly in the 0.4, 0.1 and 0.05g contours for the 0.3, 1.0 and 3.0 second Sa maps, respectively.

## **Section II: Conclusions & Recommendations**

In this section we have demonstrated that a conservative shakemap that takes the larger of two values, one calculated by deterministic integration of fault slip, and the other by a directivity sensitive attenuation relationship provides reasonable agreement with observed PGA and Sa. The attenuation model we used (Somerville et al., 1997) does not presently have regression formulas for PGV. It is recommended that a PGV relationship be constructed from the same data set used for the PGA and Sa relationships to provide a seamless 'conservative shakemap' for all of the strong motion parameters of interest.

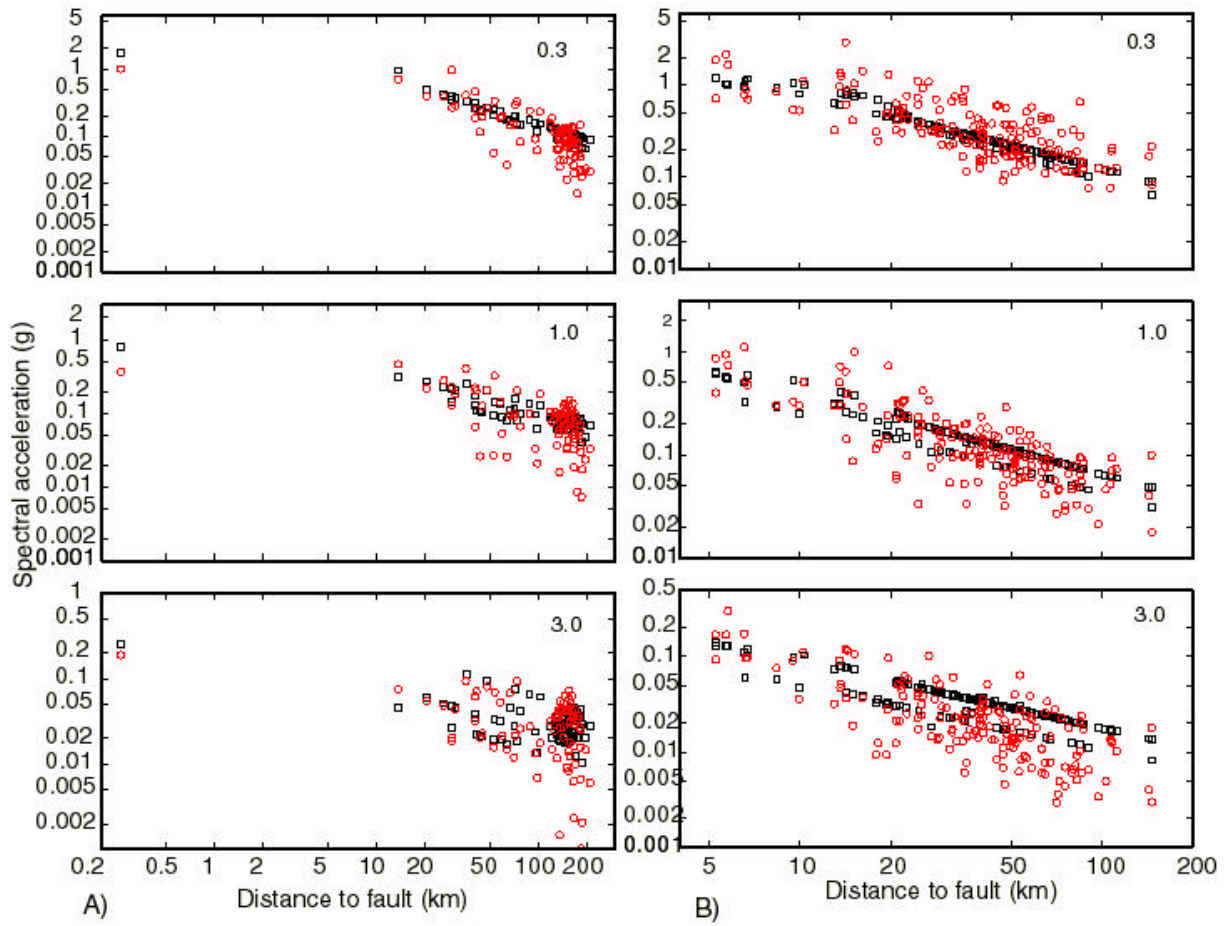
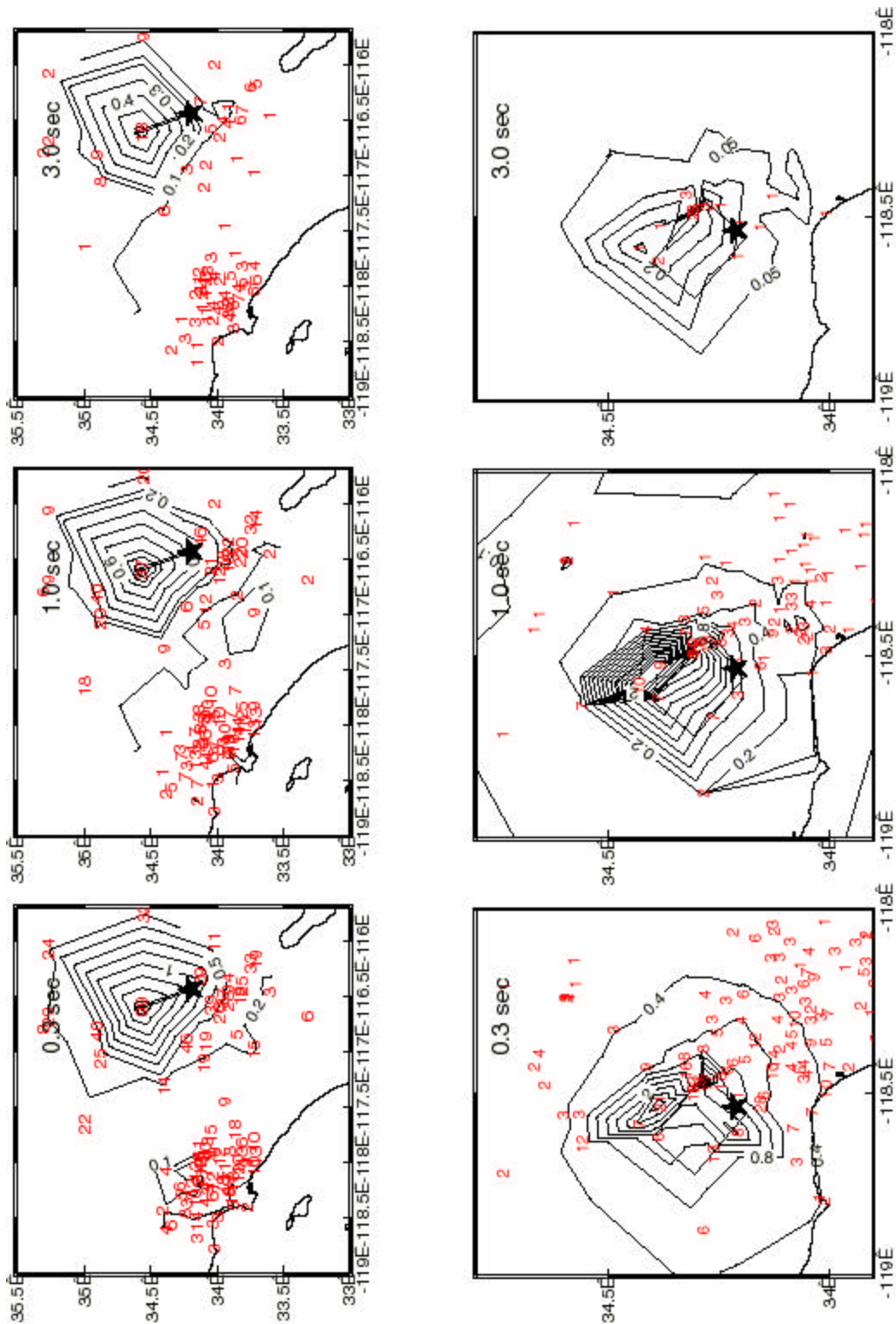


Figure 10. (a) Predicted (black squares) and observed (red circles) Sa at periods of 0.3, 1.0 and 3.0 seconds are compared for the Landers earthquake. The predicted values were obtained using the relationships of Somerville et al., (1997) and the fault orientation, scalar seismic moment and slip dimension determined in our finite source inversion. (b) Same as (a) for the Northridge earthquake.







g) are compared to observations (red numbers in tenths of a g) for the Northridge earthquake. Contour intervals are 0.4, 0.2 and 0.05 g for periods of 0.3, 1.0 and 3.0 seconds, respectively.

### Section III. Site Response Effects in Simulated Shakemaps

In this section we demonstrate the effectiveness of two different approaches of correcting for site variability. One approach involves using site classification and empirically derived adjustment factors. In this comparison we use the regional quaternary/tertiary/Mesozoic (QTM) classification developed by Park and Elrick (1998) for southern California and used in the TriNet ShakeMap (Wald et al., 1999). A regional map of QTM is used to determine site type and frequency dependent site corrections derived from Borchardt (1994) are applied to the simulated time histories. The other method involves the use of different velocity structures to develop Green's functions for varied site type. This method performed better and was used in our deterministic shakemaps presented in section II.

It is important to note that in the TriNet application the site corrections are applied to an empirically derived hard rock attenuation relationship (Joyner and Boore, 1981) and therefore the mapping from the mean hardrock response to site specific response is straightforward. The application of QTM corrections to our hard rock synthetics improves the predictions but not as much as desired.

Figure 12a illustrates the misfit between our predicted hard rock PGV and observations for the Northridge earthquake in map view. Circles show soil sites and squares show rock sites. Open circles and squares indicate that the model under predicts the observations and the filled symbols indicate the model over predicts the observations. Near the source, the predicted values are relatively good however at distance from the source we find that generally the ground motions are under predicted by as much as a factor of three at some stations. Both soil and rock sites are under predicted although the greatest misfit is for LA basin stations. Figure 12b compares the predicted-to-observed PGV ratios for the case in which the hard rock PGV were adjusted using published QTM corrections (Table 2). There is marked improvement at a number of soil sites classified mostly as quaternary or tertiary. However as the symbols in Figure 12b show the amount of under prediction remains rather high. Figure 13a compares the  $\log_{10}$  of the predicted-to-observed ratio for QTM corrected PGV. The bins show a tendency toward negative values. The red bars in Figure 13 indicate that most of the under prediction is for sites located within the LA basin. The mean  $\log_{10}$  value for LA basin sites is  $-0.48$ . Quaternary sites outside the LA basin have a mean value of  $-0.22$ , and tertiary and Mesozoic sites have mean values of  $-0.10$  and  $-0.14$  respectively. While there is substantial improvement by applying the QTM corrections to our simulated PGV there remains a systematic under prediction in the LA basin and relatively large uncertainty. It is very important to note however that this comparison does not distinguish between the relative amplitude of the PGV. It is observed that the overall misfit in the San Fernando and Northridge region, that experienced the largest ground motions, is relatively small.

Figure 12c compares the predicted-to-observed PGV ratios for the site specific Green's function simulation. This simulation is found to be significantly better than both the raw hard

rock and the QTM corrected hard rock simulations. Figure 13b compares the site specific PGV  $\log_{10}$  ratios binned according to Geomatrix site classification. This figure shows that LA basin sites remain under predicted however the distribution is skewed toward values closer to 0.0. The Geomatrix soil classifications B, C and D for sites located outside the LA basin have  $\log_{10}$  values of  $-0.02$ ,  $-0.12$  and  $-0.02$ , respectively, indicating the predictions agree well with the observations. It is curious that rock sites around the fringes of the LA basin are significantly under predicted. This may be due to improper site classification or possibly regional amplification due to the LA basin 3D structure (e.g. Olsen et al., 1995). It may be necessary to numerically develop a suite of synthetic 1D-to-3D site corrections for large-scale structures such as the LA basin.

Table 2: QTM Site Corrections

Site Type ( $V_s$ , m/s)*	Corrections for Specified Input PGA			
	< 15% g	15-25% g	25-35% g	>35% g
Mesozoic (589 m/s)				
0.1-0.5 sec. period	1.0	1.0	1.0	1.0
0.5-2.0 sec. period	1.0	1.0	1.0	1.0
Tertiary (406 m/s)				
0.1-0.5 sec. period	1.14	1.10	1.04	0.98
0.5-2.0 sec. period	1.27	1.25	1.22	1.18
Quaternary (333 m/s)				
0.1-0.5 sec. period	1.22	1.15	1.06	0.97
0.5-2.0 sec. period	1.45	1.41	1.35	1.29

\* This is a simplified table for average 30m depth site velocities by type. In the map of Park and Elrick (1998) surface velocity is mapped for the southern California region and it is possible to use more specific site velocity either know or inferred to produce period specific amplitude corrections following Borchardt (1994).

### Section III Conclusions

It is clear from the preceding comparisons that applying site specific corrections derived empirically improve results but not to the degree hoped, nor to a degree better than what is achieved when we use two 1D velocity models to represent rock and non-rock sites. There is a systematic bias toward under prediction of PGV, particularly at LA basin sites. Even rock sites along the fringes of LA basin are under predicted. This suggests that at these sites the rock velocity model (Table 1) used to compute the Green's functions is not appropriate and that 3D basin effects may be important. In fact, the work of Olsen et al. (1995) shows substantial amplification effects due to the LA basin in their finite difference simulations. Stidham et al. (1999) in their study of three dimensional wave propagation in the San Francisco bay area discovered basin amplification of as much as 3-4 over reference 1D ground motions within the tertiary basins, and more importantly that the basin amplification effects can extend beyond the boundaries of the mapped basins. Because we are using synthetic seismograms in our deterministic shakemaps it seems reasonable that we need to apply correction factors that are relative to the specific 1D model used. This can be accomplished by simulating ground motions using finite difference methods for a reference 1D velocity model and best estimate 3D structure in the Los Angeles and SF Bay Area

regions. A regional table of 1D-to-3D site corrections may be developed by considering an ensemble average of calculations for sources distributed around the region.

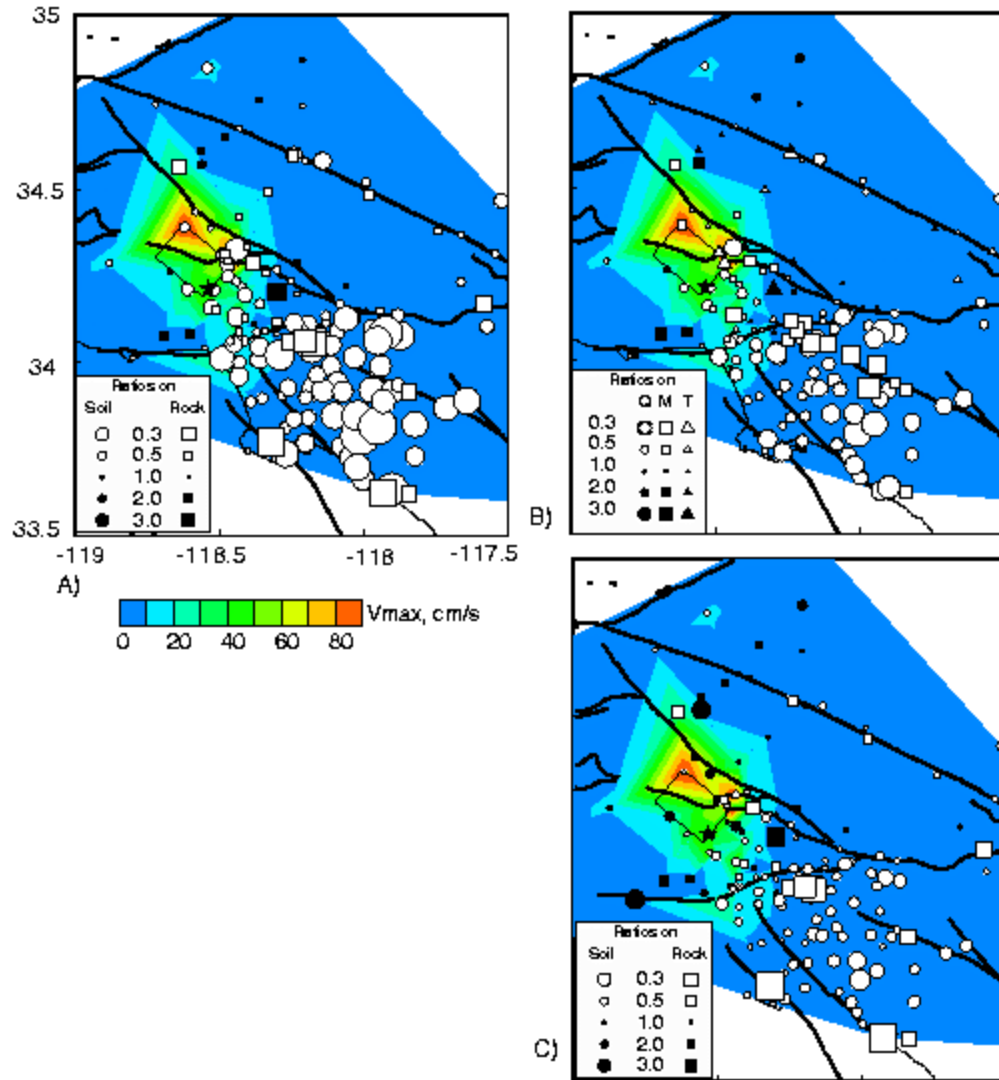


Figure 12. Predicted to observed PGV amplitude ratios for soil sites (circles) and rock sites (squares) are plotted in map view. (a) The predicted PGV were computed using the hard rock model (Table 1) and the Northridge slip (Figure 3a). (b) The predicted PGV were computed with the hard rock model (Table 1) with applied QTM corrections (Table 2). Quaternary, tertiary and Mesozoic sites are indicated by circles, squares and triangles, respectively. (c) The predicted site specific PGV were computed using both the hard rock and soil models (Table 1) and the Northridge slip (Figure 3a). In each example the size of the symbol is proportional to the predicted-to-observed ratio, and open symbols indicate under prediction and filled symbols indicate over prediction

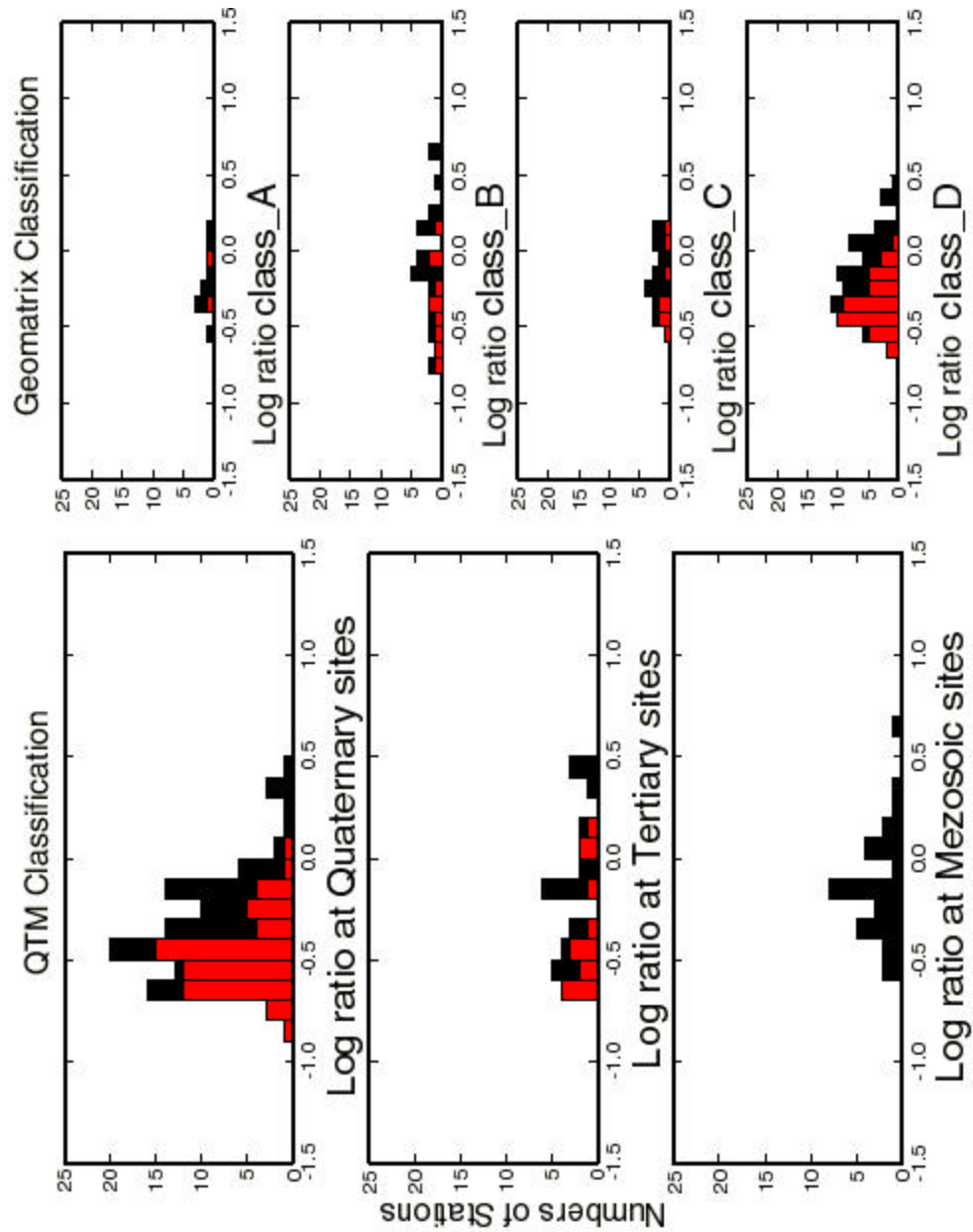


Figure 13. The  $\log_{10}$  of the predicted-to-observed PGV amplitude ratio for Northridge is compared for the case where hard rock synthetic PGV have QTM corrections (Table 2) applied (a), and the site specific PGV classified according to the Geomatrix scheme. The black bars show all stations and the red bars show stations located in the Los Angeles basin. A value of 0.0 indicates a predicted-to-observed ratio of 1.

## Section IV: Application of Data/Model Shakemaps

This report is concluded by demonstrating how our ‘conservative shakemap’ may be integrated with actual observations to produce a data/model shakemap. At the outset of this study we have been concerned with developing methodology that will perform in very sparse station coverage situations. Sparse coverage is a function of population density and there are vast areas of California with relatively sparse coverage. Recent earthquakes in southern Oregon (1993 Klamath Falls M6) and near Lake Tahoe (1994 Double Springs Flat M6) are cases in which the closest strong motion stations were located 60-80 km away. Figure 14 compares data only PGA shakemaps obtained by direct contouring of observations for the Northridge earthquake. Figure 14a shows the shakemap obtained by using only the 13 TriNet stations located in the region. This figure identifies the region of strong shaking by the 0.4g contour and compares well with the results obtained for PGV with many more stations (Figure 2b). In Figure 14b we consider a case in which strong motion station spacing is approximately 30 km with one station located in the forward directivity region. This map is successful in identifying the region of strongest shaking but the 0.4g contour is not closed. If the forward directivity station is removed it is not possible to obtain a useable PGA shakemap by contouring only data. Determination of a strong motion centroid and application of point-source attenuation models to interpolate the map improves a sparse station shakemap (e.g. Wald et al., 1999). In very sparse coverage it may be difficult to obtain a strong motion centroid that correlates with where the strongest shaking occurred.

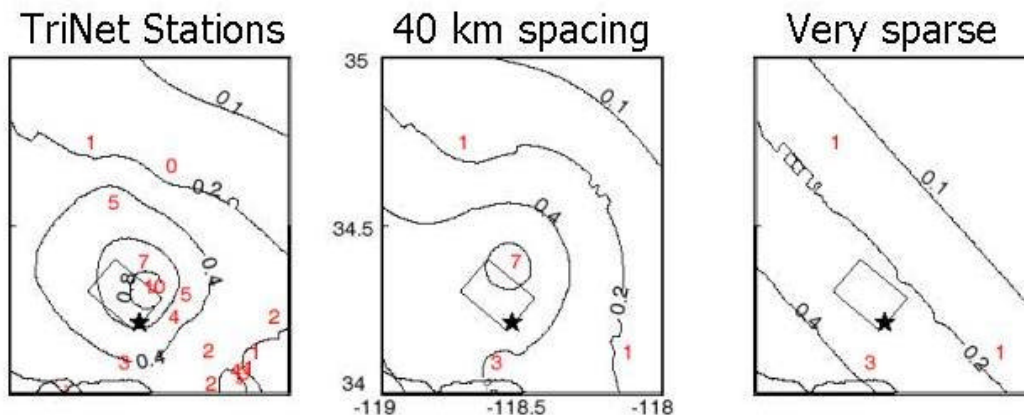


Figure 14. PGA shakemaps obtained by contouring only data values for the Northridge earthquake are compared for cases with (a) 13 nearby TriNet stations, (b) 30 km station spacing with one station located in the forward directivity region, and (c) 30 km station spacing as might be anticipated in sparsely instrumented regions or regions with few digitally telemetered strong motion stations. The contours show PGA in g and the red numbers show the observed PGA in tenths of a g that were used to develop the shakemap contours.

Figure 15 compares a combined model/data shakemap obtained using QTM adjusted hard rock simulations and the directivity sensitive attenuation model (Somerville et al., 1997). The red circles show where model predictions were incorporated in shakemap contouring. In these maps the model predictions are introduced at regular intervals only in regions where there is no observing station located within 22 km. The coarse grid of model predictions and data is then finely interpolated onto a mesh  $1/10^{\text{th}}$  of the spacing shown and contoured. At this final interpolation and contouring stage QTM corrections are applied. Observed data values are uncorrected. This is essentially the same approach outlined by Wald et al. (1999) and used in the TriNet shakemap. Figure 15a illustrates that such a map with many direct observations is controlled by the data (i.e. Figure 14a and 15a are very similar). Figures 15b and 15c show that the model contributes significantly in sparse station coverage by producing shakemaps that accurately describe the forward directivity amplification of ground motion. It is interesting that the 0.7g observation in Figure 15b pins the map at this level and therefore results in an under prediction where the 1 g PGA was observed in Figure 15a. Figure 15c, with the 0.7g observation removed actually performs better because a maximal PGA of 1 g is obtained indicating the severity of the earthquake and the resulting 0.8g contour lies near the location of the 1g observation.

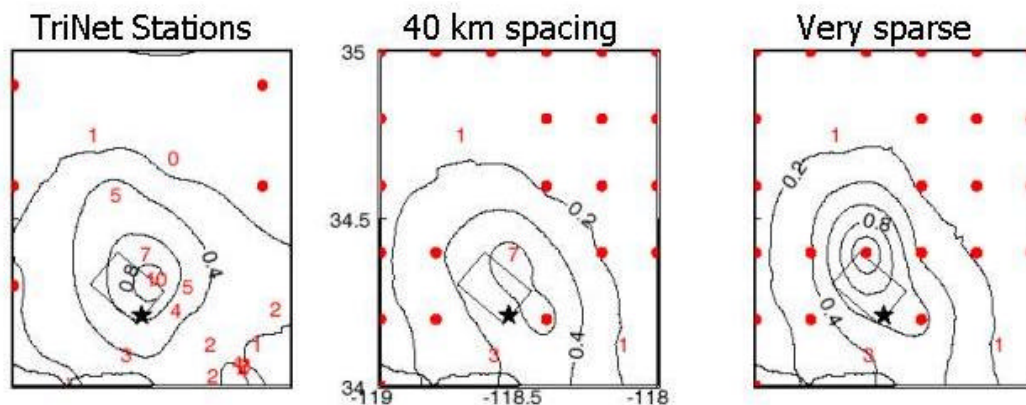


Figure 15. PGA shakemaps obtained by contouring data and model values for the Northridge earthquake are compared for cases with (a) 13 nearby TriNet stations, (b) 30 km station spacing with one station located in the forward directivity region, and (c) 30 km station spacing. The contours show PGA in g, the red numbers show the observed PGA in tenths of a g and the red circles show the locations of where model predictions were added to develop the shakemap contours.

The extended nature of the Landers earthquake is illustrated in the last example. Figure 16a and 16b compare data only PGA shakemaps with and without the near-fault LUC station. The near-fault ground motions in Figure 16a is controlled by the LUC station. When LUC is removed the near-fault ground motion is significantly under predicted when only data is contoured. Again by considering the location of a strong motion centroid and model predictions using point-source attenuation (e.g. Wald et al., 1999) the near fault predictions without LUC would be expected to be better, however the pattern would likely be similar to that in Figure 16a or Figure 2a with a central point of high ground motion. Figures 16c and 16d compare data/model PGA shakemaps for the cases with and without the LUC station. With LUC the overall map is very similar to that in Figure 16a however near the fault the

model produces an elongate region of elevated ground motions that would be expected for an extended rupture of the size experienced in the Landers earthquake. If LUC is removed (Figure 16d) the resulting map retains the elongate near-fault pattern of large PGA, and in fact the LUC site lies between the 0.5 and 0.6g contours of the map, which is a fairly good estimate of the observed 0.76g acceleration. Probably the most important lesson from Figure 16 is that it is not enough to have a single near-fault observation to characterize ground motions for a large extended rupture. A better scenario would have an array of observing stations along the length of the fault. This may be possible in densely instrumented regions, but is not practical in many areas of California. For earthquakes such as Landers, where instrumentation is relatively sparse, considering a source specific directivity model to fill in the holes in observations may result in better estimates of near fault ground motions. Unfortunately along most of the length of Landers we don't know what the actual ground motion levels were, however based on the slip models that have been published it is likely that ground motions close to that observed at LUC occurred along the whole length of the fault.

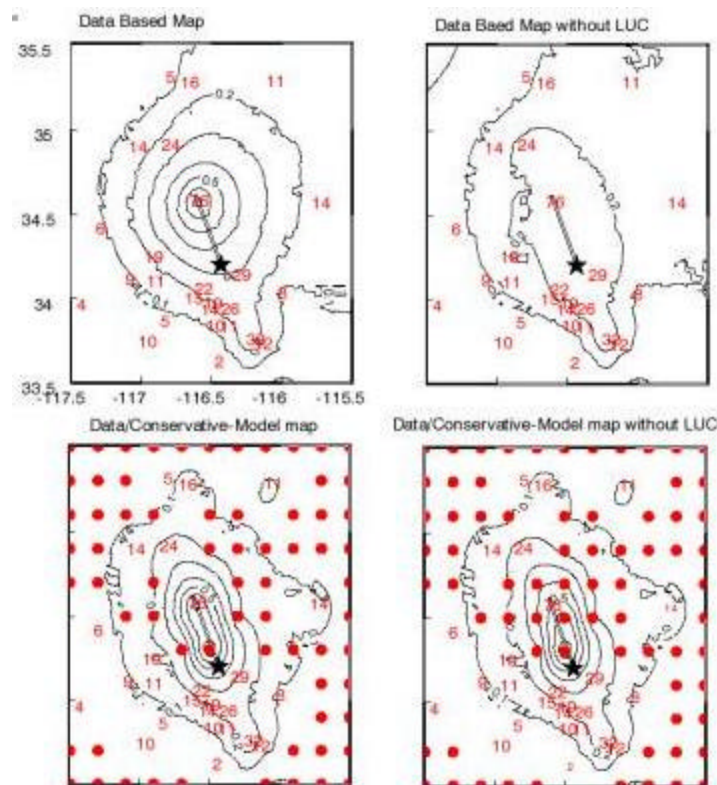


Figure 16. Data only PGA shakemaps for the Landers earthquake are compared for cases with (a) and without (b) the near-fault LUC station. These maps were obtained by direct contouring of the data shown in red (numbers in units of hundredths of a g). The contours are in units of g. The data/model shakemaps are compared for the same cases with (c) and without (d) the LUC station. The red circles show where model predictions were incorporated into the contouring process



In summary, the objectives of this study have been met and software for the determination of combined model/data shakemaps that incorporate source specific directivity effects has been developed. Comparisons of shakemaps for Landers and Northridge indicate the procedure performs well. In the coming year this method will be integrated into the offline REDI system to being testing under operational conditions.



## References

- Abercrombie, R. E. Local observations of the onset of a large earthquake; 28 June 1992 Landers, California, *Bull. Seism. Soc. Am.*, 84, 725-734.
- Borcherdt, R. D. (1994) Estimates of site-dependent response spectra for design (methodology and justification), *Earthquake Spectra*, 10, 617-653.
- Cohee, B. P., and G. C. Beroza (1994). A comparison of two methods for earthquake source inversion using strong motion seismograms, *Annali Di Geophysica*, **37**, 1515-1538.
- Dreger, D. S., and D. V. Helmberger (1991). Source Parameters of the Sierra Madre Earthquake from Regional and Local Body Waves, *Geophys. Res. Lett.*, 18, 2015-2018.
- Dreger, D. S., and D. V. Helmberger (1993), Determination of Source Parameters at Regional Distances with Single Station or Sparse Network Data, *Journ. Geophys. Res.*, 98, 8107-8125.
- Dreger, D. and B. Romanowicz (1994). Source Characteristics of Events in the San Francisco Bay Region, *USGS Open-file report*, 94-176, 301-309.
- Dreger, D. (1994a). Empirical Green's function study of the January 17, 1994 Northridge mainshock ( $M_w$  6.7), *Geophys. Res. Lett.*, **21**, 2633-2636.
- Dreger, D. S. (1994b), Investigation of the Rupture Process of the 28 June 1992 Landers Earthquake Utilizing TERRAscope, *Bull. Seism. Soc. Am.*, 84, 713-724.
- Dreger, D. (1997), The Large Aftershocks of the Northridge Earthquake and their Relationship to Mainshock Slip and Fault Zone Complexity, *Bull. Seism. Soc. Am.*, 87, 1259-1266.
- Gee, L. S., D. S. Neuhauser, D. S. Dreger, M. Pasyanos, R. A. Uhrhammer, and B. Romanowicz (1996), Real-Time Seismology at UC Berkeley: The Rapid Earthquake Data Integration Project, *Bull. Seism. Soc. Am.*, 86, 936-945.
- Heaton, T. H. (1990) Evidence for and implications of self-healing pulses of slip in earthquake rupture, *Phys. Earth and Planet. Int.*, 64, 1-20.
- Joyner, B. and D. Boore (1981) Peak horizontal accelerations and velocity from strong-motion records including records from the 1979 Imperial Valley, California, earthquake, *Bull. Seism. Soc. Am.*, 71, 2011-2038.
- Olsen, K. B., R. J. Archuleta, and J. R. Matarese (1995) Three-dimensional simulation of a magnitude 7.75 earthquake on the San Andreas Fault, *Science*, 270, 1628-1632.
- Park, S., and S. Elrick (1998) Predictions of shear-wave velocities in southern California using surface geology, *Bull. Seism. Soc. Am.*, 88, 677-685.
- Pasyanos, M. E., D. S. Dreger, and B. Romanowicz (1996), Towards Real-Time Determination of Regional Moment Tensors, *Bull. Seism. Soc. Am.*, 86, 1255-1269.

- Pitarka, A., P. Somerville, Y. Fukushima, T. Uetake, K. Irikura (1999) Simulation of near-fault strong ground motion using hybrid Green's functions, submitted to Bull. Seism. Soc. Am.
- Saikia, C. (1994) Modified frequency-wavenumber algorithm for regional seismograms using Filon's quadrature; modeling of  $L_g$  waves in eastern North America, Geophys. Journ. Int., 118, 142-158.
- Somerville, P. G., N. F. Smith, R. W. Graves, and N. A. Abrahamson (1997) Modification of empirical strong ground motion attenuation relations to include the amplitude and duration effects of rupture directivity, Seism. Res. Lett., 68, 199-222.
- Stidham, C., M. Antolik, D. Dreger, S. Larsen and B. Romanowicz (1999) Three-dimensional structure influences on the strong motion wavefield of the 1989 Loma Prieta earthquake, in press Bull. Seism. Soc. Am.
- Wald, D. J., V. Quitoriano, T. H. Heaton, H. Kanamori, C. W. Scrivner, and C. B. Worden (1999) TriNet "ShakeMaps": Rapid Generation of Instrumental Ground Motion and Intensity Maps for Earthquakes in Southern California, in press Earthquake Spectra.
- Wald, D. J., and T. H. Heaton (1994). Spatial and temporal distribution of slip for the 1992 Landers, California, earthquake, *Bull. Seism. Soc. Am.*, **84**, 668-691.
- Wald, D. J., T. H. Heaton, and K. W. Hudnut (1996). The slip history of the 1994 Northridge, California, earthquake determined from strong-motion, teleseismic, GPS, and leveling data, *Bull. Seism. Soc. Am.*, **86**, s49-s70.
- Wells, D. L., and K. J. Coppersmith (1994) New empirical relationships among magnitude, rupture length, rupture width, rupture area, and surface displacement, Bull. Seism. Soc. Am., 84, 974-1002.
- Zeng, Y., J. G. Anderson, and G. Yu (1994) A composite source model for computing realistic synthetic strong ground motions, Geophys. Res. Lett., 21, 725-728.
- Zeng, Y., and J. G. Anderson (1996). A composite source model of the 1994 Northridge earthquake using genetic algorithms, *Bull. Seism. Soc. Am.*, 86, s71-s83.

## Acknowledgements

The work described in this report was funded by the Pacific Earthquake Engineering Research (PEER) Center under the Pacific Gas & Electric Company Contract No. 09566. This financial support is gratefully acknowledged.

The financial support of the PEARL sponsor organizations including the Pacific Gas & Electric Company (PG&E), the California Energy Commission (CEC), and the California Department of Transportation (Caltrans) is acknowledged.

This work was supported in part by the Pacific Earthquake Engineering Research Center through the Earthquake Engineering Research Centers Program of the National Science Foundation under Award number EEC-9701568.

## **ACKNOWLEDGEMENTS**

The work described in this report was funded by the Pacific Earthquake Engineering Research (PEER) Center under the Pacific Gas & Electric Company Contract No. 09566. This financial support is gratefully acknowledged.

The financial support of the PEARL sponsor organizations including the Pacific Gas & Electric Company (PG&E), the California Energy Commission (CEC), and the California Department of Transportation (Caltrans) is acknowledged.

This work was supported in part by the Pacific Earthquake Engineering Research Center through the Earthquake Engineering Research Centers Program of the National Science Foundation under Award number EEC-9701568.